ORIGINAL PAPER

A novel electrochemiluminescence biosensor based on the self-ECL emission of conjugated polymer dots for lead ion detection

Ying He[1] · Xiaoxia Hu[1] · Zhengjun Gong[2] · Shihong Chen[1] · Ruo Yuan[1]

Abstract

The poly[(9,9-dioctylfuorenyl-2,7-diyl)-alt-co-(1,4-benzo-{2,1′,3}-thiadiazole)] (PFBT) was carboxyl-functionalized to prepare polymer dots (C-PFBT Pdots), which served as a self-ECL emitter for producing an extraordinary ECL signal without any exogenous coreactants. The C-PFBT Pdots–modified electrode captured the substrate DNA and further hybridized with a ferrocene (Fc)-labeled DNA. The ECL emission of C-PFBT Pdots was quenched by Fc (a signal off state). After the DNAzyme was added, the DNAzyme-substrate hybrids were formed through hybridizing between DNAzyme and substrate and the Fc-labeled DNA was released. In the presence of target Pb^{2+}, the DNAzyme-substrate hybrids could be specifically recognized and cleaved to release the DNAzyme and Pb^{2+}. Ultimately, the released DNAzyme would further hybridize with the substrate for producing the DNAzyme-substrate hybrids and then were cleaved by the released Pb^{2+}. As a result, the DNA walking machine was generated and the substantial Fc was away from C-PFBT Pdots to obtain a signal on state. Such a strategy achieved a sensitive detection of Pb^{2+} and the detection limit was as low as 0.17 pM. Moreover, making this ECL biosensor for an intracellular Pb^{2+} detecting, a convincing performance was achieved. The self-ECL emitter C-PFBT Pdots combining with the quencher Fc provided a new strategy and platform for constructing a coreactant-free ECL assay.

Keywords Self-electrochemiluminescence · C-PFBT Pdots · Biosensor · DNA · Lead ions

Introduction

Electrochemiluminescence (ECL), as a kind of electrochemistry-merged luminescence [1], has aroused increasing concerns in bio-research and environmental monitoring because of its high sensitivity, low background interference, electrochemical controllability, and excellent selectivity

✉ Zhengjun Gong
  gongzhengjun@126.com

✉ Shihong Chen
  cshong@swu.edu.cn

1 Chongqing Engineering Laboratory of Nanomaterials & Sensor Technologies, College of Chemistry and Chemical Engineering, Southwest University, Chongqing 400715, People's Republic of China

2 Faculty of Geosciences and Environmental Engineering, Southwest Jiaotong University, Chengdu 611756, China

[2, 3]. The ECL technology has been widely applied for detecting the protein, nucleic acid, and small biomolecules, such as dopamine and glucose. For example, our group constructed an ECL ratiometric biosensor to achieve a highly sensitive determination of dopamine [4]. The Khalilzadeh's group developed an ECL aptamer-based biosensor for the determination of thrombin [5]. Besides, Liu and co-workers applied a bipedal DNA walker signal amplification strategy to construct an ECL biosensor for detecting miRNA-21 [6]. The ECL has provided a sensitive strategy for biological analysis.

The ECL emission usually involved two pathways, namely, the annihilation-based pathway and coreactant-based pathway. The annihilation-based ECL emission usually produced a low ECL efficiency, which made a trace analysis difficult to be implemented. Multitudinous ECL systems for biological analysis usually relied on a coreactant-based pathway to obtain enough detection sensitivity since the coreactant could remarkably enhance the ECL emission of luminophores [7–9]. However, as we know, a coreactant-dependent ECL detection would encounter various confusions no matter what strategy is used to apply the coreactant. For example, the direct addition of exogenous coreactant in a testing solution may

destroy the detection microenvironment, and lead to a poor detection stability and reproducibility [10]. The immobilization of coreactants at the sensing interface may introduce complex operations. Furthermore, the immobilized coreactants may encounter a leakage from the sensing interface. Regarding the dissolved oxygen as coreactant, the uncertainty of dissolved oxygen concentration also would make the system lack the stability and repeatability. Considering the confusions from the application of coreactants, constructing a self-ECL system excluding the application of external coreactants and dissolved oxygen is essential.

In order to construct a self-ECL system for an actual analysis, the selection of self-ECL emitter and suitable ECL signal switching mode is crucial. Traditional ECL luminophores, such as organic emitters [11], metallic complex [12], quantum dots [13], and metal nanoclusters [14] generally needed external coreactants or dissolved oxygen to achieve high luminescence intensity. The polyfluorene, as a new kind of luminophore, exhibited a remarkable brightness, high emission rate, and extraordinary photostability, thus receiving an extensive interest in the ECL biosensing and imaging [15, 16]. Based on the application of coreactants H_2O_2, $C_2O_4^{2-}$, or tripropylamine (TPrA), the highly sensitive detection of choline [17], melamine [16], and cancer biomarkers [18] was achieved. More importantly, the polyfluorene has been recently found to exhibit an extraordinary self-ECL property without any external species and dissolved oxygen as conreactants, which endowed the polyfluorene an extensive application prospect in the construction of ECL sensing. For instance, our group proposed an ECL strategy to detect the nucleic acid by coupling carboxyl-functionalized PFBT dots as a self-ECL emitter and black hole (BHQ) as an effective quencher [19]. Ma and co-workers achieved the detection of nitroaromatics with poly [9,9-bis(3′-(N,N-dimethylamino) propyl)-2,7-fluorene]-alt-2,7 -(9,9-dioctylfluorene)] (PFN) as the self-ECL emitter and aluminum tris(8-quinolinolate) as the quencher [20]. However, the ECL resonance energy transfer (ECL-RET) between the self-ECL emitter and quencher was involved in the signal switching process, namely the ECL-RET between PFBT and BHQ, and between PFN and aluminum tris(8-quinolinolate). The ECL-RET-based signal switching mode would limit the application of above self-ECL systems due to the distance dependence of ECL-RET. Thus, developing a self-ECL system excluding the ECL-RET was of great significance.

Lead ions (Pb^{2+}), as a major environmental pollutant, are harmful to the human body even at extremely low levels (100 mg/L in blood), including the hematological, cardiovascular, neurological, gastrointestinal, and renal system [21]. Thus, the rapid and accurate detection of Pb^{2+} in environmental and biological samples is particularly important and urgently demanded. Many traditional methods for Pb^{2+} detection have been developed, including high-performance liquid chromatography, atomic absorption/emission spectrometry, inductively coupled plasma-mass spectrometry, and inductively coupled plasma-atomic emission spectrometry, which have an acceptable sensitivity and accuracy [22–25]. Nevertheless, the ECL technology has received an extensive attention in Pb^{2+} detection due to its superiority in overcoming the expensive instruments, sophisticated sample preparation, or time-consuming procedures of the above-mentioned methods [26–28]. For example, Zhu et al. applied the $Ru(bpy)_3^{2+}$-TPA system to achieve an ECL detection of Pb^{2+} [26]. Li et al. used CdS quantum dots/H_2O_2 ECL system to construct an ECL sensor for Pb^{2+} detection [28]. Although the ECL technology offers more possibilities for the sensitive detection of Pb^{2+}, the ECL systems reported so far generally involved external species or dissolved oxygen as coreactants and the toxic and instability may be resulted from their application [11, 18]. Therefore, developing a self-ECL-sensing platform for Pb^{2+} excluding ECL-RET was very valuable.

In this work, an ECL biosensor was constructed for detecting Pb^{2+} with C-PFBT Pdots as self-ECL emitter and Fc as quencher. As exhibited in Scheme 1, C-PFBT Pdots–modified glassy carbon electrode (GCE) produced a strong ECL signal. C-PFBT Pdots served as a matrix for immobilizing the substrate DNA and further captured the DNA 1 labeled with Fc to obtain a "signal-off" state since Fc and C-PFBT Pdots were brought into close proximity for making the ECL signal of C-PFBT Pdots be quenched by Fc. With the introduction of DNAzyme, the DNAzyme chain hybridized with the substrate chain to form a stable duplex, accompanied with the release of Fc-labled DNA 1. In the presence of Pb^{2+}, the DNA duplex formed by the DNAzyme chain and substrate chain selectively recognized Pb^{2+}. Then the ribonucleotides (rA) in the substrate chain were cleaved and Pb^{2+} was released. Meanwhile, the DNAzyme chain would hybridize with the adjacent complete substrate chain. Once again, the released Pb^{2+} was identified by the DNA duplex to circularly activate the next DNAzyme. As a result, the DNAzyme chain continuously walked along the substrate chain modified on the electrode and the Fc-labeled DNA 1 was released, namely forming a DNA walking machine, which recovered the ECL signal of C-PFBT Pdots to obtain a "signal-on" state, thus achieving the detection of Pb^{2+}. The designed self-ECL strategy exhibited a good performance in the detection of Pb^{2+} in MB-231 and A-549 cells. Such a self-ECL assay excluding ECL-RET would provide an attractive ECL platform for the biological analysis.

Experimental

Reagents, chemicals, and apparatus

The information on reagents, chemicals, and apparatus in this work has been described in the Supplementary Materials.

Scheme 1 Schematic illustration of **a** the preparation of C-PFBT Pdots and **b** the fabrication of the biosensor
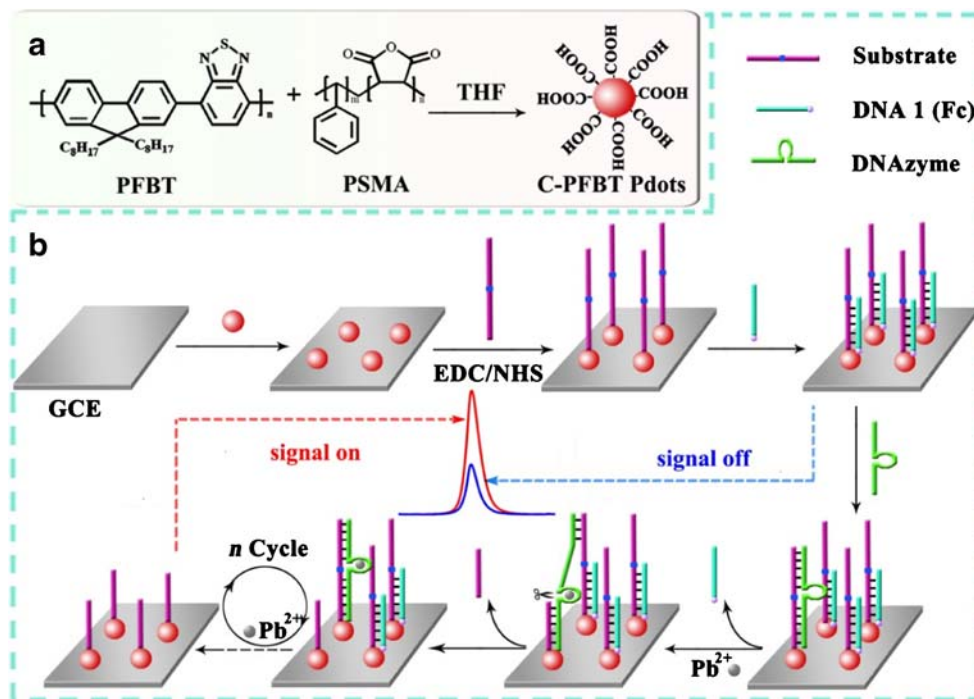
Preparation of the C-PFBT Pdots

Firstly, PFBT and poly (styrene-co-maleicanhydride) (PSMA) were dissolved in THF to achieve a stock solution (1.0 mg/mL), respectively. Subsequently, the prepared PFBT (4 mL) and PSMA (800 μL) solutions were mixed and sonicated for producing a homogeneous solution. The resulting solution was quickly added into 10 mL ultrapure water. Ultimately, the THF was evaporated under vacuum with a constant stirring to obtain C-PFBT Pdots. The synthesis process of C-PFBT Pdots is shown in Scheme 1a.

Fabrication of the ECL biosensor

After polishing and cleaning the glassy carbon electrode (GCE, $\Phi = 4.0$ mm) [29], 10-μL dispersion of C-PFBT Pdots was coated on the surface of GCE. After dried in air, the obtained C-PFBT Pdots/GCE was incubated with 0.02 g/mL of EDC and 0.01 g/mL of NHS for 30 min. Then, the electrode was incubated with 2 μL of substrate DNA (50 μM) at 4 °C for overnight and further incubated with 2 μL of DNA1 (50 μM) at room temperature for 2 h. Finally, 2 μL of DNAzyme (50 μM) and Pb^{2+} with various concentrations were incubated onto the electrode surface at room temperature for 140 min. The construction of ECL biosensor is depictured in Scheme 1b.

Native polyacrylamide gel electrophoresis

The operation of PAGE analysis is displayed in the Supplementary Materials.

Results and discussion

### Characterization of the C-PFBT Pdots

Figure 1a exhibits the SEM images of C-PFBT Pdots, and a clear spherical structure was observed, which is similar to the previous report [19], demonstrating the successful synthesis of C-PFBT Pdots. Figure 1b presents the size distribution of C-PFBT Pdots, and the average particle diameter of C-PFBT Pdots was about 68 nm.

ECL behavior of the self-ECL system

The effect of dissolved O_2 on the ECL emission of C-PFBT Pdots was firstly studied. As seen from Fig. 2a, in both cases, namely in air-saturated PBS solution (0.10 M pH 7.4) (curve a) and N_2-saturated PBS solution (0.10 M pH 7.4) (curve b), the ECL signals were almost identical, indicating that the dissolved O_2 was excluded from the ECL reaction of C-PFBT Pdots.

Secondly, the effect of testing mediums including PBS solution and MeCN solution was also monitored. In the case of MeCN solution, $TBAPF_6$ served as the supporting electrolyte. The ECL signal of C-PFBT Pdots/GCE was detected in PBS solution (0.10 M, pH 7.4) and MeCN solution, respectively. As seen from Fig. 2a, the modified electrode displayed a remarkably decreased ECL signal in MeCN solution (Fig. 2a, curve c), as compared with that in PBS solution (Fig. 2a, curve a), indicating a vital role of the aqueous solution in the ECL emission.

Fig. 1 **a** SEM images of C-PFBT Pdots. **b** Size distribution of C-PFBT Pdots
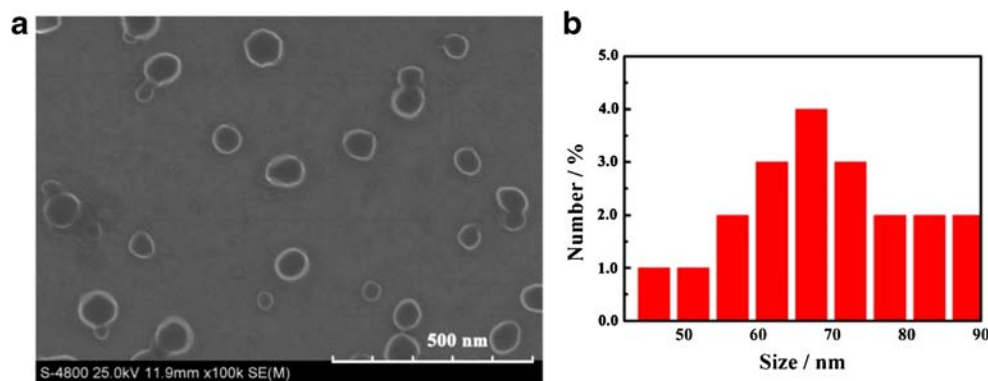
Since the vital role of aqueous solution was observed, the effects of reactive oxygen species (ROS) including the hydroxyl radical (OH$^\cdot$) and superoxide radical (O$_2^{\cdot-}$) in aqueous solution were explored. The L-cysteine (L-cys) and superoxide dismutase (SOD) were introduced to eliminate OH$^\cdot$ and O$_2^{\cdot-}$, and Fig. 2a presents the results. As seen, the ECL signal at C-PFBT Pdots/GCE with L-cys (curve d) or SOD (curve e) was almost identical to that without L-cys and SOD (curve a), illustrating that OH$^\cdot$ and O$_2^{\cdot-}$ did not participate in the ECL reaction of C-PFBT Pdots.

To further elucidate the possible ECL mechanisms of C-PFBT Pdots without any exogenous coreactants, the effect of pH was explored and Fig. 2b depictures the results. As seen, the C-PFBT Pdots–modified electrode displayed a constantly increased ECL signal with increasing pH from 1 to 11, demonstrating the decisive role of OH$^-$ in the ECL emission. The possible self-ECL mechanisms for C-PFBT Pdots may be summarized as follows. Firstly, the oxidation of C-PFBT Pdots occurred on the electrode surface, and the radical cation C-PFBT Pdots$^{\cdot+}$ was generated. The radical cation reacted with OH$^-$ to produce the reducing intermediate radical C-PFBT Pdots$^{\cdot}$. Then, the excited state C-PFBT Pdots* was yield when C-PFBT Pdots$^{\cdot}$ encountered with C-PFBT Pdots$^{\cdot+}$, thereby occurring the self-ECL emission, as reported by the previous literature [19].

Polyacrylamide gel electrophoresis analysis

The feasibility of the DNA reaction on the electrode was verified by polyacrylamide gel electrophoresis (PAGE). Fig. S1 illustrates the results. The distinct bands in lanes 1–3 corresponded to the DNA1, substrate DNA, and DNAzyme, respectively. With the hybridization between DNA1 and substrate DNA, a brightened band appeared (lane 4). After the DNAzyme was introduced, an additionally slower migrate band was observed (lane 5), suggesting that the hybrids of DNAzyme and substrate DNA were formed and the DNA1 was released. After Pb^{2+} was introduced, a new and obvious band appeared (lane 6), which corresponded to the short chain DNA released during the Pb^{2+} cleaving, and it migrated the fastest. The above PAGE results verified the formation of DNA walking machine during the detection of Pb^{2+} at the biosensor.

CV, EIS, and ECL characterization of the modified electrode

CV characterization of each modification step was conducted in PBS (0.10 M, pH 7.4) in the presence of K$_3$[Fe(CN)$_6$]/K$_4$[Fe(CN)$_6$] (5.0 mM) as the supporting electrolyte and Fig. 3a depictures the results. Compared with the bare GCE (curve a), the C-PFBT Pdots–modified GCE displayed an

Fig. 2 **a** The ECL response of C-PFBT Pdots/GCE in PBS (0.10 M pH 7.4) with (a) air-satuarted and (b) N$_2$-satuarted, (c) in MeCN solution under air-saturated, in PBS (0.10 M pH 7.4) containing (d) L-cys and (e) SOD. **b** ECL response of C-PFBT Pdots/GCE in PBS (0.10 M pH 7.4) with pH from 1 to 11. Scanning potential range, 0~1.25 V; scanning rate, 300 mV/s
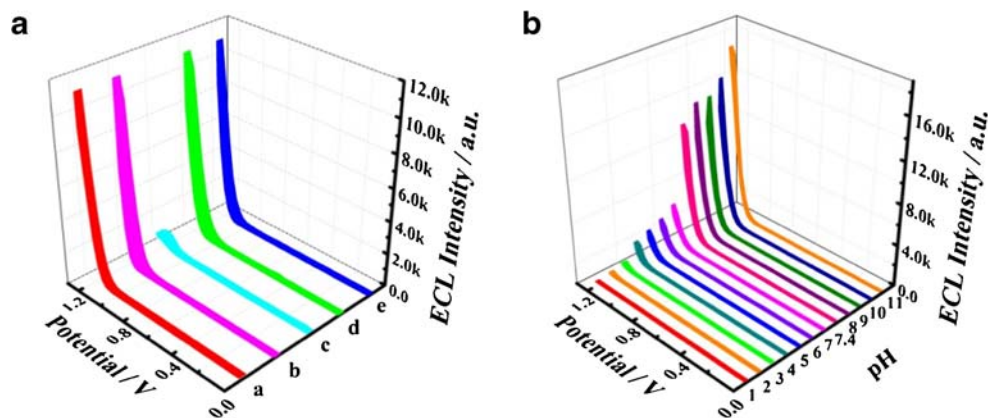
Fig. 3 a CV and **b** EIS diagrams of (a) bare GCE, (b) C-PFBT Pdots/GCE, (c) C-PFBT Pdots/GCE with substrate and Fc-labeled DNA 1, (d) C-PFBT Pdots/GCE with substrate, DNAzyme and Pb^{2+} in 5.0 mM $[Fe(CN)_6]^{3-/4-}$ solution. The insert of **b**: the equivalent circuit. The effect of **c** pH of PBS solution and **d** incubation time of Pb^{2+} on the ECL response at the biosensor. Scanning potential range of $-0.2\sim0.6$ V and scanning rate of 100 mV/s for CV detection. The init potential of 0.22 V, amplitude of 5 mV, and frequency of $0.1\sim10^5$ Hz for EIS detection. Scanning potential range of $0\sim1.25$ V and scanning rate of 300 mV/s for ECL detection
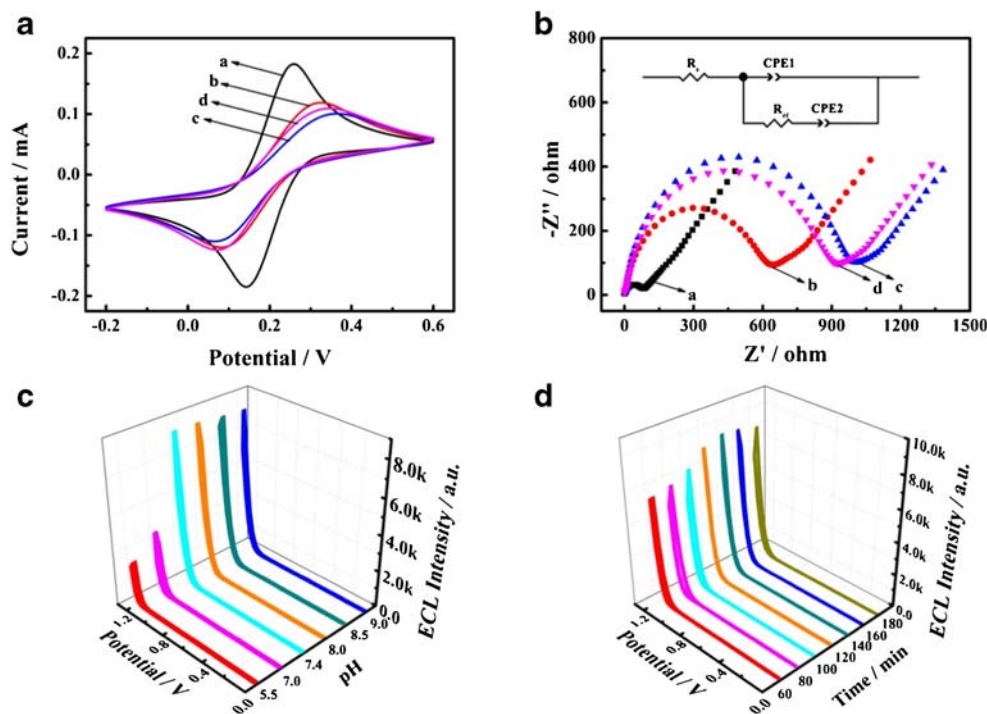
obviously decreased redox peak current (curve b), which was ascribed to the resistance of C-PFBT Pdots to the electron transfer. As the C-PFBT Pdots/GCE was successively incubated with the substrate DNA and Fc-labeled DNA 1, a further decreased redox peak current was observed (curve c). After the DNA walking machine was triggered by DNAzyme and Pb^{2+}, the Fc-labeled DNA 1 was released from the electrode surface, and the redox peak current was enhanced again (curve d).

The EIS characterization was also performed with the $[Fe(CN)_6]^{3-}/[Fe(CN)_6]^{4-}$ as a redox probe. The impedance spectra are pictured as the Nyquist plots (Fig. 3b), and their high-frequency regions exhibited a semicircle. The diameter of the semicircle was equal to the impedance of electron transfer (R_{et}). As seen, a relatively small R_{et} was detected at a bare GCE (curve a). When C-PFBT Pdots were modified onto the

surface of GCE, the R_{et} evidently increased due to the non-conductive of C-PFBT Pdots nanomaterial (curve b). After the substrate DNA and Fc-labeled DNA 1 were successively incubated onto the surface of C-PFBT Pdots/GCE, a further increased R_{et} was observed because the biomolecules blocked the electron transfer (curve c). When the DNA walking machine was triggered by DNAzyme and Pb^{2+}, a decreased R_{et} was detected (curve d). Additionally, the insert pictures are the equivalent circuit of impedance spectra. EIS results indicated a successful construction of the biosensor.

Additionally, ECL measurements of each modification step were further conducted in PBS (0.10 M, pH 7.4). No ECL signal was detected at a bare GCE (Fig. S2, curve a). As expectedly, the C-PFBT Pdots modified electrode exhibited a strong ECL response (Fig. S2, curve b). With the introduction of Fc-labeled DNA 1 (Fig. S2, curve c), the ECL signal was quenched by Fc, which was mainly ascribed to the electron transport between Fc and C-PFBT Pdots. Finally, when Fc was away from the surface of electrode with the generation of DNA walking machine triggered by target Pb^{2+}, an increased ECL signal was obtained (Fig. S2, curve d).

Optimization of experimental conditions

The incubation time of Pb^{2+} and pH of PBS solution were optimized in the case of 1.0×10^{-4} M Pb^{2+}. Firstly, the pH of PBS was optimized and Fig. 3c displays the results. The ECL intensity gradually increased as pH shifted from 5.5 to 7.4 and reached a maximum at pH 7.4. As pH exceeded 7.4, a gradually decreased ECL signal was observed with increasing

Table 1 Comparison of this constructed ECL assay with other methods

Detection method	Detection limit	Linear range	Reference
Fluorescence	5.0 nM	20–1000 nM	[32]
Fluorescence	0.3 nM	0.1–100 μM	[33]
Fluorescence	10 nM	10 nM–10 μM	[34]
Fluorescence	0.03 nM	0.1–50 nM	[35]
Fluorescence	20 nM	100–4000 nM	[36]
Colorimetry	13 nM	0.03–2 μM	[37]
Electrochemical	0.6 nM	1.51–302 nM	[38]
Electrochemical	21 nM	25–1000 nM	[39]
ECL	0.167 nM	0.5 pM–5 mM	This work

Fig. 4 **a** ECL response of the biosensor towards different concentrations of Pb^{2+}, from a to h: 5.0×10^{-10}, 5.0×10^{-9}, 5.0×10^{-8}, 5.0×10^{-7}, 1.0×10^{-7}, 1.0×10^{-6}, 1.0×10^{-5}, and 1.0×10^{-4} M, respectively. **b** Linear calibration between the ECL intensity and the logarithm of Pb^{2+} concentration. Scanning potential, 0~1.25 V; scanning rate, 300 mV/s
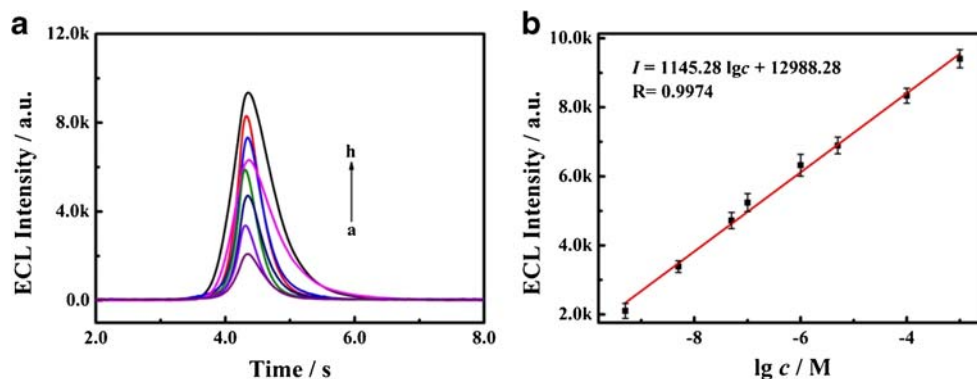

pH from 7.4 to 9.0, which was mainly ascribed to the fact that the nucleic acid strand showed the maximum activity at a physiological pH. Therefore, the optimal pH of 7.4 was used in subsequent experiments. Secondly, the incubation time of Pb^{2+} was optimized and Fig. 3d presents the results. When the cleaving time of target Pb^{2+} ranged from 50 to 200 min, the ECL signal increased first and then decreased accordingly and reached the maximum at 140 min. Therefore, the incubation time of target Pb^{2+} in subsequent experiments was chosen as 140 min.

Analytical performance of the biosensor

The quantitative detection of Pb^{2+} was performed at the constructed biosensor under the optimized experimental conditions. As seen from Fig. 4a, as the concentration of Pb^{2+}

ranged from 0.5 pM to 0.1 mM, the ECL intensity gradually increased. The increase in ECL signals was ascribed to the departure of the ECL quencher Fc labeled in the DNA 1 from the electrode's surface, which was triggered by Pb^{2+}. And a good liner relationship between the ECL intensity and the logarithm of Pb^{2+} concentration was obtained with a linear regression equation $I = 12{,}988.28 + 1145.28 \lg c$ ($R = 0.9974$) (Fig. 4b). Here, I and c stand for the ECL intensity and the concentration of Pb^{2+}, respectively. Based on the IUPAC recommendations [30, 31], the limit of detection (LOD) of 0.17 pM was obtained. Our proposed biosensor was compared with other strategies for Pb^{2+} detection and the results are illustrated in Table 1. Compared with reported detection platforms, our constructed ECL system exhibited a higher sensitivity for quantifying Pb^{2+}.

Fig. 5 **a** ECL response of the biosensor to 0.10 μM Pb^{2+} in 0.10 M PBS (pH 7.4) under the continuous cyclic scans. **b** ECL response of the biosensor towards the blank (a), 0.10 mM of Hg^{2+}, Cu^{2+}, Mg^{2+}, Mn^{2+}, Ni^{2+}, Cd^{2+}, Co^{2+} (from b to h), 0.10 μM Pb^{2+} (i), and the mixture of Pb^{2+} and interferences (j). **c** The inter-assay and intra-assay of four biosensors in the presence of 0.10 μM Pb^{2+} in 0.10 M PBS (pH 7.4). **d** Calibration curve of ECL intensity vs the logarithmic concentrations of intracellular Pb^{2+} from MB-231 (red line) and A-549 (blue line). Scanning potential, 0~1.25 V; scanning rate, 300 mV/s
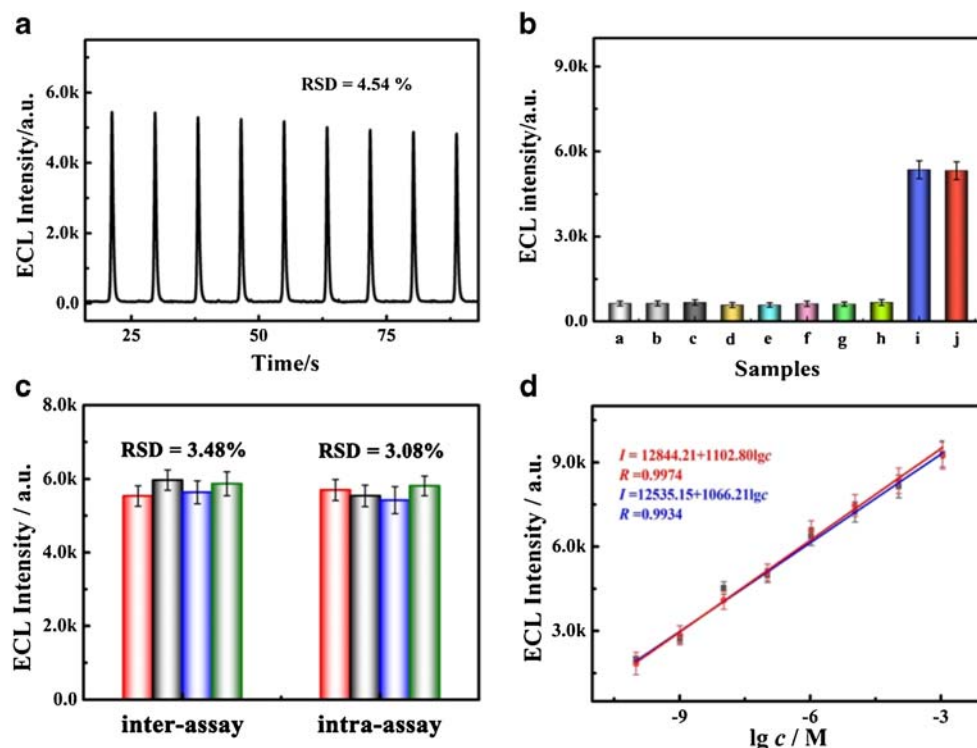
Stability, selectivity, and reproducibility studies

The consecutive cyclic potential scans at the biosensor were performed to evaluate the stability of the biosensor. As depicted in Fig. 5a, the relative standard deviation (RSD) of 4.54% was obtained for the ECL intensity in the case of the consecutive cyclic potential scans for 9 cycles at 0.10 μM of Pb^{2+}, demonstrating a good stability of the biosensor. Some possible interferences including Hg^{2+}, Cu^{2+}, Mg^{2+}, Mn^{2+}, Ni^{2+}, Cd^{2+}, and Co^{2+} were chosen to evaluate the selectivity of our proposed self-ECL assay. As seen from Fig. 5b, no obvious ECL response was observed in the case of 1.0 mM interferences (from b to h), as compared with the blank (a). However, in the case of 0.10 μM Pb^{2+} (i), the biosensor presented a strong ECL response. Moreover, the ECL response towards the mixture of 0.10 μM Pb^{2+} and 1.0 mM interferences (j) was almost the same as that of Pb^{2+} alone (i), suggesting a high selectivity of our proposed ECL biosensor for Pb^{2+} detection. The intra- and inter-assays were explored to evaluate the reproducibility of the biosensor, and Fig. 5c depicts the results. As seen, four biosensors from the different or the same batch did not exhibit any obvious change in the ECL response towards 0.10 μM Pb^{2+}, indicating an acceptable reproducibility for Pb^{2+} detection.

Analysis of real samples

To estimate the practical applicability of our developed ECL biosensor, the MB-231 cells and A-549 cells were selected as models and were cultured in DMEM medium containing different concentrations of Pb^{2+}. After being cultured with Pb^{2+}, the MB-231 cells and A-549 cells were washed with the DMEM medium without Pb^{2+} for removing the Pb^{2+} adsorbed on the cells' surface. Then, the cell lysates were prepared and further employed to perform the ECL measurements using our developed biosensors. The preparation of cell lysates was described in the Supplementary Materials. The Pb^{2+} in cell lysates of MB-231 cells and A-549 cells was firstly measured with the inductively coupled plasma-mass spectrometry (ICP-MS). As expected, for two different cell lines, an excellent linear relationship was observed between the ECL signal strength and the logarithm of intracellular Pb^{2+} concentration (Fig. 5d). Furthermore, the calibration plots for two different cell lines almost overlap, demonstrating a potential application of our designed coreactant-free ECL strategy.

Conclusion

A self-ECL biosensor was designed for the ultrasensitive detection of Pb^{2+} based on C-PFBT Pdots as the self-ECL emitter and Fc as the quencher. Firstly, such a self-ECL system successfully overcame the disadvantage of introducing exogenous coreactants. Secondly, the combination of excellent ECL performance of C-PFBT Pdots and high quenching efficiency of Fc endowed this signal on-off-on strategy a low background signal and high detection sensitivity for Pb^{2+}. Thirdly, the specific cyclic cleaves of Pb^{2+} achieved target recycling and enhanced the selectivity of the biosensor. Moreover, the designed biosensor demonstrated a preliminary application in the determination of intracellular Pb^{2+}. The self-ECL system provided a new strategy and platform for ECL sensing and imaging technologies without any exogenous coreactants and the ECL-RET.

Compliance with ethical standards

Conflict of interest The authors declare that they have no competing interests.

References

1. Zhang H, Zuo FM, Tan XR, Xu SH, Yuan R, Chen SH (2018) A novel electrochemiluminescent biosensor based on resonance energy transfer between poly(9,9-di- n -octylfluorenyl-2,7-diyl) and 3,4, 9,10-perylenetetracar-boxylic acid for insulin detection. Biosens Bioelectron 104:65–71

2. Richter MM (2004) Electrochemiluminescence (ECL). Chem Rev 104(6):3003–3036

3. Khalilzadeh B, Shadjou N, Afsharan H, Eakandani M, Charoudeh HN, Rashidi MR (2016) Reduced graphene oxide decorated with gold nanoparticle as signal amplification element on ultra-sensitive electrochemiluminescence determination of caspase-3 activity and apoptosis using peptide based biosensor. BioImpacts 6(3):135–147

4. Fu XM, Tan XR, Yuan R, Chen SH (2017) A dual-potential electrochemiluminescence ratiometric sensor for sensitive detection of dopamine based on graphene-CdTe quantum dots and self-enhanced Ru(II) complex. Biosens Bioelectron 90:61–68

5. Isildak I, Navaeipour F, Afsharan H, Kanberoglu GS, Agir I, Ozer T, Annabi N, Totu EE, Khalilzadeh B (2020) Electrochemiluminescence methods using CdS quantum dots in aptamer-based thrombin biosensors: a comparative study. Microchim Acta 187:25

6. Liu W, Chen AY, Li SK, Peng KF, Chai YQ, Yuan R (2019) Perylene derivative/luminol nanocomposite as a strong electrochemiluminescence emitter for construction of an ultrasensitive MicroRNA biosensor. Anal Chem 91:1516–1523

7. Gai QQ, Wang DM, Huang RF, Liang XX, Wu HL, Tao XY (2018) Distance-dependent quenching and enhancing of electrochemiluminescence from tris(2, 2′-bipyridine) ruthenium (II)/tripropylamine system by gold nanoparticles and its sensing applications. Biosens Bioelectron 118:80–87

8. Yang F, Zhong X, Jiang XY, Zhuo Y, Yuan R, Wei SP (2019) An ultrasensitive aptasensor based on self-enhanced Au nanoclusters as highly efficient electrochemiluminescence indicator and multi-site landing DNA walker as signal amplification. Biosens Bioelectron 130:262–268

9. Zhang XL, Li WM, Zhou Y, Chai YQ, Yuan R (2019) An ultrasensitive electrochemiluminescence biosensor for MicroRNA detection based on luminol-functionalized Au NPs@ZnO nanomaterials as signal probe and dissolved O2 as coreactant. Biosens Bioelectron 135:8–13

10. Wang Y, Lu J, Tang LH, Chang HX, Li JH (2009) Graphene oxide amplified electrogenerated chemiluminescence of quantum dots and its selective sensing for glutathione from thiol-containing compounds. Anal Chem 81(23):9710–9715

11. Liu JL, Tang ZL, Zhuo Y, Chai YQ, Yuan R (2017) Ternary electrochemiluminescence system based on rubrene microrods as luminophore and Pt nanomaterials as coreaction accelerator for ultrasensitive detection of MicroRNA from cancer cells. Anal Chem 89(17):9108–9115

12. Xiong CY, Liang WB, Zheng YN, Zhuo Y, Chai YQ, Yuan R (2017) Ultrasensitive assay for telomerase activity via self-enhanced electrochemiluminescent ruthenium complex doped metal–organic frameworks with high emission efficiency. Anal Chem 89(5):3222–3227

13. Chen WL, Zhu Q, Tang QH, Zhao K, Deng AP, Li JG (2018) Ultrasensitive detection of diclofenac based on electrochemiluminescent immunosensor with multiple signal amplification strategy of palladium attached graphene oxide as bioprobes and ceria doped zinc oxide as substrates. Sensors Actuators B Chem 268:411–420

14. Zhou Y, Wang HJ, Zhang H, Chai YQ, Yuan R (2018) Programmable modulation of copper nanoclusters electrochemiluminescence via DNA nanocranes for ultrasensitive detection of microRNA. Anal Chem 90(5):3543–3549

15. Wang NN, Feng YQ, Wang YW, Ju HX, Yan F (2018) Electrochemiluminescent imaging for multi-immunoassay sensitized by dual DNA amplification of polymer dot signal. Anal Chem 90(12):7708–7714

16. Lu QY, Zhang JJ, Wu YY, Chen SH (2015) Conjugated polymer dots/oxalate anodic electrochemiluminescence system and its application for detecting melamine. RSC Adv 5(78):63650–63654

17. Chen HM, Lu QY, Liao JY, Yuan R, Chen SH (2016) Anodic electrogenerated chemiluminescence behavior and the choline biosensing application of blue emitting conjugated polymer dots. Chem Commun 52(45):7276–7279

18. Wang NN, Wang YW, Ju HX, Yan F (2018) Electrochemiluminescent imaging for multi-immunoassay sensitized by dual DNA amplification of polymer dot signal. Anal Chem 90(12):7708–7714

19. Luo JH, Li Q, Chen SH, Yuan R (2019) Coreactant-free dual amplified electrochemiluminescent biosensor based on conjugated polymer dots for the ultrasensitive detection of MicroRNA. ACS Appl Mater Interfaces 11(30):27363–27370

20. Ma L, Wu N, Liu Y, Ran X Q, Xiao D B (2019) Self-electrochemiluminescence of poly[9,9-bis(3′-(N,N- dimethyl amino)propyl)-2,7-fluorene]-alt- 2,7-(9,9- dioctylfluorene)] and resonance energy transfer to aluminum tris(8-quinolinolate). Electrochim Acta 297: 826–832

21. Childhood Lead Poisoning (2017)

22. Gao ZB, Ma XG (2011) Speciation analysis of mercury in water samples using dispersive liquid–liquid microextraction combined with high-performance liquid chromatography. Anal Chim Acta 702(1):50–55

23. Liu JS, Chen HW, Mao XQ, Jin X (2000) Determination of trace copper, lead, cadmium, and iron in environmental and biological samples by flame atomic absorption spectrometry coupled to flow injection on-line coprecipitation preconcentration using DDTC-nickel as coprecipitate carrier. Int J Environ Anal Chem 76(4): 267–282

24. Mandlate JS, Soares BM, Seeger TS, Vecchia PD, Mello PA, Flores EM, Duarte F (2017) Determination of cadmium and lead at sub-ppt level in soft drinks: an efficient combination between dispersive liquid-liquid microextraction and graphite furnace atomic absorption spectrometry. Food Chem 221:907–912

25. Uden P, Boaky HT, Kahakachchi C, Hafezi R, Nolibos P, Block E, Johnson S, Tyson JF (2004) Element selective characterization of stability and reactivity of selenium species in selenized yeast. J Anal At Spectrom 19(1):65

26. Zhu X, Lin ZY, Chen LF, Qiu B, Chen GN (2009) A sensitive and specific electrochemiluminescent sensor for lead based on DNAzyme. Chem Commun 40:6050

27. Dong YQ, Tian WR, Ren SY, Dai RP, Chi YW, Chen GN (2014) Graphene quantum dots/l-cysteine coreactant electrochemiluminescence system and its application in sensing lead(II) ions. ACS Appl Mater Interfaces 6(3):1646–1651

28. Li M, Kong QK, Bian ZQ, Ma C, Ge SG, Zhang Y, Yu JH, Yan M (2015) Ultrasensitive detection of lead ion sensor based on gold nanodendrites modified electrode and electrochemiluminescent quenching of quantum dots by electrocatalytic silver/zinc oxide coupled structures. Biosens Bioelectron 65:176–182

29. Chen HM, Zhang H, Yuan R, Chen SH (2017) Novel double-potential electrochemiluminescence ratiometric strategy in enzyme-based inhibition biosensing for sensitive detection of organophosphorus pesticides. Anal Chem 89(5):2823–2829

30. Buck RP, Lindner E (1994) Recommendations for nomenclature of ionselective electrodes (IUPAC recommendations 1994). Pure Appl Chem 66:2527–2536

31. Long GL, Winefordner JD (1983) Limit of detection. A closer look at the IUPAC definition. Anal Chem 55(7):712A–724A

32. Li T, Dong S, Wang EK (2010) A lead (II)-driven DNA molecular device for turn-on fluorescence detection of lead (II) ion with high selectivity and sensitivity. J Am Chem Soc 132:13156–13157

33. Wen ZB, Liang WB, Zhuo Y, Xiong CY, Zheng YN, Yuan R, Chai YQ (2017) An efficient target-intermediate recycling amplification strategy for ultrasensitive fluorescence assay of intracellular lead ions. Chem Commun 53:7525–7528

34. Yu Z, Zhou W, Han J, Li YC, Fan LZ, Li XH (2016) Na+ induced conformational change of Pb2+-stabilized G quadruplex and its influence on Pb2+ detection. Anal Chem 88:9375–9380

35. Peng X, Liang WB, Wen ZB, Xiong CY, Zheng YN, Chai YQ, Yuan R (2018) Ultrasensitive fluorescent assay based on a rolling-circleamplification-assisted multisite-strand-displacement-reaction signal-amplification strategy. Anal Chem 90:7474–7479

36. Xia J, Lin M, Zuo X, Su S, Wang L, Huang W, Fan C, Huang Q (2014) Metal ion-mediated assembly of DNA nanostructures for cascade fluorescence resonance energy transfer-based fingerprint analysis. Anal Chem 86:7084–7087

37. Yu YM, Hong Y, Gao P, Nazeeruddin MK (2016) Glutathione modified gold nanoparticles for sensitive colorimetric detection of Pb2+ ions in rainwater polluted by leaking perovskite solar cells. Anal Chem 88:12316–12322

38. Sun QW, Wang JK, Tang MH, Huang LM, Zhang ZY, Liu C, Lu XH, Hunter KW, Chen GS (2017) A new electrochemical system based on a flow-field shaped solid electrode and 3D-printed thin-layer flow cell: detection of Pb2+ ions by continuous flow accumulation square-wave anodic stripping voltammetry. Anal Chem 89: 5024–5029

39. Kang WJ, Pei X, Rusinek CA, Bange A, Haynes EN, Heineman WR, Kang IP (2017) Determination of lead with a copper-based electrochemical sensor. Anal Chem 89:3345–3352